

Rotating Electroweak Sphaleron-Antisphaleron Systems

Rustam Ibadov

*Department of Theoretical Physics and Computer Science,
Samarkand State University, Samarkand, Uzbekistan*

Burkhard Kleihaus, Jutta Kunz and Michael Leissner

Institut für Physik, Universität Oldenburg, D-26111 Oldenburg, Germany

(Dated: November 16, 2018)

At finite weak mixing angle the sphaleron solution of Weinberg-Salam theory can be endowed with angular momentum proportional to the electric charge. Here we show, that this holds also for sphaleron-antisphaleron systems such as pairs, chains and vortex rings. We also address the equilibrium conditions for these solutions.

PACS numbers: 14.80.Hv, 11.15Kc

I. INTRODUCTION

The electroweak sector of the standard model harbours unstable non-perturbative classical solutions: sphalerons [1–4]. The static sphaleron solution of Weinberg-Salam theory represents the top of the energy barrier between topologically inequivalent vacua. Since the standard model does not absolutely conserve baryon number [5, 6], at finite temperature baryon number violating processes can arise because of thermal fluctuations of the fields large enough to overcome the energy barrier between distinct vacua. The rate for baryon number violating processes is then largely determined by a Boltzmann factor, containing the height of the barrier at a given temperature [7–10]. The sphaleron itself carries baryon number $Q_B = 1/2$ [2].

At finite weak mixing angle the static electroweak sphaleron possesses a large magnetic moment but does not carry electric charge. As argued before [11] and demonstrated recently in nonperturbative studies [12, 13], the addition of electric charge leads to a non-vanishing Poynting vector and thus a finite angular momentum density of the system. Consequently a branch of spinning electrically charged sphalerons arises. Since these carry non-vanishing baryon number as well, they also entail baryon number violating processes.

Beside the sphaleron, the non-trivial topology of the configuration space of Weinberg-Salam theory gives rise to further unstable classical solutions. A superposition of n sphalerons, for instance, can lead to static axially symmetric solutions, multisphalerons, which carry baryon number $Q_B = n/2$ and whose energy density is torus-like [14–16]. A superposition of a sphaleron and an antisphaleron, on the other hand, can give rise to a bound sphaleron-antisphaleron system, in which a sphaleron and an antisphaleron are located at an equilibrium distance on the symmetry axis [17–19]. Such a sphaleron-antisphaleron pair has vanishing baryon number, $Q_B = 0$, since the antisphaleron carries $Q_B = -1/2$. The sphaleron-antisphaleron pair therefore does not mediate baryon number violating processes.

Recently, the sphaleron-antisphaleron pair solutions have been generalized, to form sphaleron-antisphaleron chains, where m sphalerons and antisphalerons are located on the symmetry axis, in static equilibrium [20], in close analogy to the monopole-antimonopole chains encountered in the Georgi-Glashow model [21]. When multisphalerons and -antisphalerons are considered instead, vortex ring solutions arise, when $n \geq 3$ [20], where the Higgs field vanishes not (only) on isolated points on the symmetry axis but (also) on one or more rings, centered around the symmetry axis [22, 23].

Here we consider the addition of electric charge to such multisphaleron and sphaleron-antisphaleron systems. As for the simple sphaleron, the non-vanishing Poynting vector leads to a finite angular momentum density for these configurations. Thus branches of rotating electrically charged sphalerons emerge from the respective static electrically neutral configurations. We construct these solutions explicitly and discuss their properties. The angular momentum and the electric charge of the solutions are proportional [12, 20, 24].

In section 2 we present the action, the Ansatz and the boundary conditions. In section 3 we consider the relevant physical properties and, in particular, derive the linear relation between angular momentum and electric charge. We present and discuss the numerical results in section 4. These include global properties of the solutions, such as their energy, their angular momentum, their charge and their magnetic moments, but also local properties, such as their energy density, their angular momentum density and the modulus of their Higgs field. Moreover, we discuss the equilibrium conditions for the solutions. We give our conclusions in section 5.

II. ACTION AND ANSATZ

We consider the bosonic sector of Weinberg-Salam theory

$$\mathcal{L} = -\frac{1}{2}\text{Tr}(F_{\mu\nu}F^{\mu\nu}) - \frac{1}{4}f_{\mu\nu}f^{\mu\nu} - (D_\mu\Phi)^\dagger(D^\mu\Phi) - \lambda(\Phi^\dagger\Phi - \frac{v^2}{2})^2 \quad (1)$$

with su(2) field strength tensor

$$F_{\mu\nu} = \partial_\mu V_\nu - \partial_\nu V_\mu + ig[V_\mu, V_\nu], \quad (2)$$

su(2) gauge potential $V_\mu = V_\mu^a\tau_a/2$, u(1) field strength tensor

$$f_{\mu\nu} = \partial_\mu A_\nu - \partial_\nu A_\mu, \quad (3)$$

and covariant derivative of the Higgs field

$$D_\mu\Phi = \left(\partial_\mu + igV_\mu + i\frac{g'}{2}A_\mu\right)\Phi, \quad (4)$$

where g and g' denote the $SU(2)$ and $U(1)$ gauge coupling constants, respectively, λ denotes the strength of the Higgs self-interaction and v the vacuum expectation value of the Higgs field.

The gauge symmetry is spontaneously broken due to the non-vanishing vacuum expectation value of the Higgs field

$$\langle\Phi\rangle = \frac{v}{\sqrt{2}}\begin{pmatrix} 0 \\ 1 \end{pmatrix}, \quad (5)$$

leading to the boson masses

$$M_W = \frac{1}{2}gv, \quad M_Z = \frac{1}{2}\sqrt{(g^2 + g'^2)}v, \quad M_H = v\sqrt{2\lambda}. \quad (6)$$

$\tan\theta_w = g'/g$ determines the weak mixing angle θ_w , defining the electric charge $e = g\sin\theta_w$. We also denote the weak fine structure constant $\alpha_W = g^2/4\pi$.

To obtain stationary rotating solutions of the bosonic sector of Weinberg-Salam theory, we employ the time-independent axially symmetric Ansatz

$$V_\mu dx^\mu = \left(B_1 \frac{\tau_r^{(n,m)}}{2g} + B_2 \frac{\tau_\theta^{(n,m)}}{2g}\right) dt - n \sin\theta \left(H_3 \frac{\tau_r^{(n,m)}}{2g} + H_4 \frac{\tau_\theta^{(n,m)}}{2g}\right) d\varphi + \left(\frac{H_1}{r} dr + (1 - H_2) d\theta\right) \frac{\tau_\varphi^{(n)}}{2g}, \quad (7)$$

$$A_\mu dx^\mu = (a_1 dt + a_2 \sin^2\theta d\varphi) / g', \quad (8)$$

and

$$\Phi = i \left(\phi_1 \tau_r^{(n,m)} + \phi_2 \tau_\theta^{(n,m)}\right) \frac{v}{\sqrt{2}} \begin{pmatrix} 0 \\ 1 \end{pmatrix}. \quad (9)$$

where

$$\begin{aligned} \tau_r^{(n,m)} &= \sin m\theta(\cos n\varphi\tau_x + \sin n\varphi\tau_y) + \cos m\theta\tau_z, \\ \tau_\theta^{(n,m)} &= \cos m\theta(\cos n\varphi\tau_x + \sin n\varphi\tau_y) - \sin m\theta\tau_z, \\ \tau_\varphi^{(n)} &= (-\sin n\varphi\tau_x + \cos n\varphi\tau_y), \end{aligned}$$

n and m are integers, and τ_x , τ_y and τ_z denote the Pauli matrices.

The two integers n and m determine the type of configuration, that is put into rotation. For $n = m = 1$ the solutions correspond to rotating sphalerons. Rotating multisphaleron configurations arise for $n > 1$ and $m = 1$. For $n = 1$ and $m > 1$ rotating sphaleron-antisphaleron pairs ($m = 2$) or sphaleron-antisphaleron chains arise, and for $n \geq 3$ rotating vortex ring solutions.

The ten functions B_1 , B_2 , H_1, \dots, H_4 , a_1 , a_2 , ϕ_1 , and ϕ_2 depend on r and θ , only. With this Ansatz the full set of field equations reduces to a system of ten coupled partial differential equations in the independent variables r and θ . A residual $U(1)$ gauge degree of freedom is fixed by the condition $r\partial_r H_1 - \partial_\theta H_2 = 0$ [3].

Requiring regularity and finite energy, we impose for odd m configurations the boundary conditions

$$\begin{aligned}
r = 0 : \quad & B_1 \sin m\theta + B_2 \cos m\theta = 0, \quad \partial_r (B_1 \cos m\theta - B_2 \sin m\theta) = 0, \quad H_1 = H_3 = H_4 = 0, \quad H_2 = 1, \\
& \partial_r a_1 = 0, \quad a_2 = 0, \quad \phi_1 = 0, \quad \phi_2 = 0 \\
r \rightarrow \infty : \quad & B_1 = \gamma \cos m\theta, \quad B_2 = \gamma \sin m\theta, \quad H_1 = H_3 = 0, \quad H_2 = 1 - 2m, \quad H_4 = \frac{2 \sin m\theta}{\sin \theta}, \\
& a_1 = \gamma, \quad a_2 = 0, \quad \phi_1 = 1, \quad \phi_2 = 0, \quad \text{where } \gamma = \text{const.} \\
\theta = 0 : \quad & \partial_\theta B_1 = 0, \quad B_2 = 0, \quad H_1 = H_3 = 0, \quad \partial_\theta H_2 = \partial_\theta H_4 = 0, \quad \partial_\theta a_1 = \partial_\theta a_2 = 0, \quad \partial_\theta \phi_1 = 0, \quad \phi_2 = 0, \quad (10)
\end{aligned}$$

where the latter hold also at $\theta = \pi/2$, except for $B_1 = 0$ and $\partial_\theta B_2 = 0$. For even m configurations the same set of boundary conditions holds except for

$$\begin{aligned}
r = 0 : \quad & \phi_1 \sin m\theta + \phi_2 \cos m\theta = 0, \quad \partial_r (\phi_1 \cos m\theta - \phi_2 \sin m\theta) = 0 \\
\theta = \pi/2 : \quad & \partial_\theta B_1 = 0, \quad B_2 = 0, \quad \partial_\theta H_3 = 0, \quad H_4 = 0. \quad (11)
\end{aligned}$$

III. GLOBAL CHARGES OF SPHALERON-ANTISPHALERON SYSTEMS

We now address the global charges of the sphaleron-antisphaleron systems, their mass, their angular momentum, their electric charge, and their baryon number. The mass M and angular momentum J are defined in terms of volume integrals of the respective components of the energy-momentum tensor. The mass is obtained from

$$M = - \int T_t^t d^3r, \quad (12)$$

while the angular momentum

$$J = \int T_\varphi^t d^3r = \int \left[2\text{Tr} (F^{t\mu} F_{\varphi\mu}) + f^{t\mu} f_{\varphi\mu} + 2 (D^t \Phi)^\dagger (D_\varphi \Phi) \right] d^3r \quad (13)$$

can be reexpressed with help of the equations of motion and the symmetry properties of the Ansatz [24–27] as a surface integral at spatial infinity

$$J = \int_{S_2} \left\{ 2\text{Tr} \left(\left(V_\varphi - \frac{n\tau_z}{2g} \right) F^{rt} \right) + \left(A_\varphi - \frac{n}{g'} \right) f^{rt} \right\} r^2 \sin \theta d\theta d\varphi. \quad (14)$$

The power law fall-off of the $U(1)$ field of a charged solution allows for a finite flux integral at infinity and thus a finite angular momentum. Insertion of the asymptotic expansion for the $U(1)$ field

$$\begin{aligned}
a_1 &= \gamma - \frac{\chi}{r} + O\left(\frac{1}{r^2}\right), \\
a_2 &= \frac{\zeta}{r} + O\left(\frac{1}{r^2}\right), \quad (15)
\end{aligned}$$

and of the analogous expansion for the $SU(2)$ fields then yields for the angular momentum

$$\frac{J}{4\pi} = \frac{n\chi}{g^2} + \frac{n\chi}{g'^2} = \frac{n\chi}{g^2 \sin^2 \theta_w} = \frac{n\chi}{e^2}. \quad (16)$$

The field strength tensor $\mathcal{F}_{\mu\nu}$ of the electromagnetic field \mathcal{A}_μ ,

$$\mathcal{A}_\mu = \sin \theta_w V_\mu^3 + \cos \theta_w A_\mu, \quad (17)$$

as given in a gauge where the Higgs field asymptotically tends to Eq. (5), then defines the electric charge \mathcal{Q}

$$\mathcal{Q} = \int_{S_2} * \mathcal{F}_{\theta\varphi} d\theta d\varphi = 4\pi \left\{ \frac{\sin \theta_w \chi}{g} + \frac{\cos \theta_w \chi}{g'} \right\} = 4\pi \frac{\chi}{e}, \quad (18)$$

where the integral is evaluated at spatial infinity. Comparison of Eqs. (16) and (18) then yields a linear relation between the angular momentum J and the electric charge \mathcal{Q} [12, 13]

$$J = \frac{n\mathcal{Q}}{e}. \quad (19)$$

This relation corresponds to the relation for monopole-antimonopole systems without magnetic charge [28]. The magnetic moment μ is obtained from the asymptotic expansion Eq. (15), analogously to the electric charge,

$$\mu = \frac{4\pi\zeta}{e}. \quad (20)$$

Addressing finally the baryon number Q_B , its rate of change is given by

$$\frac{dQ_B}{dt} = \int d^3r \partial_t j_B^0 = \int d^3r \left[\vec{\nabla} \cdot \vec{j}_B + \frac{1}{32\pi^2} \epsilon^{\mu\nu\rho\sigma} \left\{ g^2 \text{Tr}(F_{\mu\nu} F_{\rho\sigma}) + \frac{1}{2} g'^2 f_{\mu\nu} f_{\rho\sigma} \right\} \right]. \quad (21)$$

Starting at time $t = -\infty$ at the vacuum with $Q_B = 0$, one obtains the baryon number of a sphaleron solution at time $t = t_0$ [2],

$$Q_B = \int_{-\infty}^{t_0} dt \int_S \vec{K} \cdot d\vec{S} + \int_{t=t_0} d^3r K^0, \quad (22)$$

where the $\vec{\nabla} \cdot \vec{j}_B$ term is neglected, and the anomaly term is reexpressed in terms of the Chern-Simons current

$$K^\mu = \frac{1}{16\pi^2} \epsilon^{\mu\nu\rho\sigma} \left\{ g^2 \text{Tr} \left(F_{\nu\rho} V_\sigma - \frac{2}{3} i g V_\nu V_\rho V_\sigma \right) + \frac{1}{2} g'^2 f_{\nu\rho} A_\sigma \right\}. \quad (23)$$

In a gauge, where

$$V_\mu \rightarrow \frac{i}{g} \partial_\mu \hat{U} \hat{U}^\dagger, \quad \hat{U}(\infty) = 1, \quad (24)$$

\vec{K} vanishes at infinity. Subject to the above ansatz and boundary conditions the baryon charge of the sphaleron solution [15, 29] is then

$$Q_B = \int_{t=t_0} d^3r K^0 = \frac{n(1 - (-1)^m)}{4}. \quad (25)$$

IV. RESULTS AND DISCUSSION

We have solved the set of ten coupled non-linear elliptic partial differential equations numerically [30], subject to the above boundary conditions in compactified dimensionless coordinates, $x = \tilde{r}/(1 + \tilde{r})$, with $\tilde{r} = gvr$. Restricting to $M_H = M_W$, and employing the physical value for the mixing angle θ_w , we have performed a systematic study of the rotating sphaleron-antisphaleron systems with $1 \leq m \leq 6$ and $1 \leq n \leq 6$.

Starting from a given static neutral solution for a sphaleron-antisphaleron system characterized by the integers n and m , we have constructed the corresponding branch of rotating solutions, by slowly increasing the asymptotic value of the parameter $\tilde{\gamma} = \gamma/gv$, which specifies the boundary conditions for the time components of the gauge fields. The rotating branch ends when the limiting value $\tilde{\gamma}_{\max} = 1/2$ is reached [36]. Here some of the gauge field functions no longer decay exponentially. This therefore precludes localized solutions for larger values of $\tilde{\gamma}$.

A. Multisphalerons

We first present our results for the rotating multisphaleron solutions, i.e., the branches of rotating solutions with $m = 1$ and $n > 1$. We exhibit in Fig. 1a the asymptotic gauge field parameter $\tilde{\gamma} = \gamma/gv$ versus the scaled angular momentum of multisphaleron solutions consisting of n superposed sphalerons with $1 \leq n \leq 6$. Since the angular momentum J increases with n , we exhibit the angular momentum per sphaleron J/n , choosing units of $J_0 = 4\pi/g^2$. As $\tilde{\gamma}$ increases from zero to its maximal value $\tilde{\gamma}_{\max} = 1/2$, the angular momentum increases monotonically. Consequently the solutions have maximal spin at $\tilde{\gamma}_{\max}$.

Considering the increase of the angular momentum with the number of sphalerons n , we note that this increase is faster than linear. Thus the value of the maximal angular momentum per sphaleron, J_{\max}/n increases with n . The more sphalerons a configuration consists of, the more angular momentum the constituents can contribute.

Let us next consider the linear relation (19) between the charge Q and the angular momentum J . According to this relation, we should obtain a single straight line, when exhibiting the charge versus the scaled angular momentum per sphaleron, J/n . We demonstrate this in Fig. 1b, where we exhibit the charge parameter χ (which is proportional

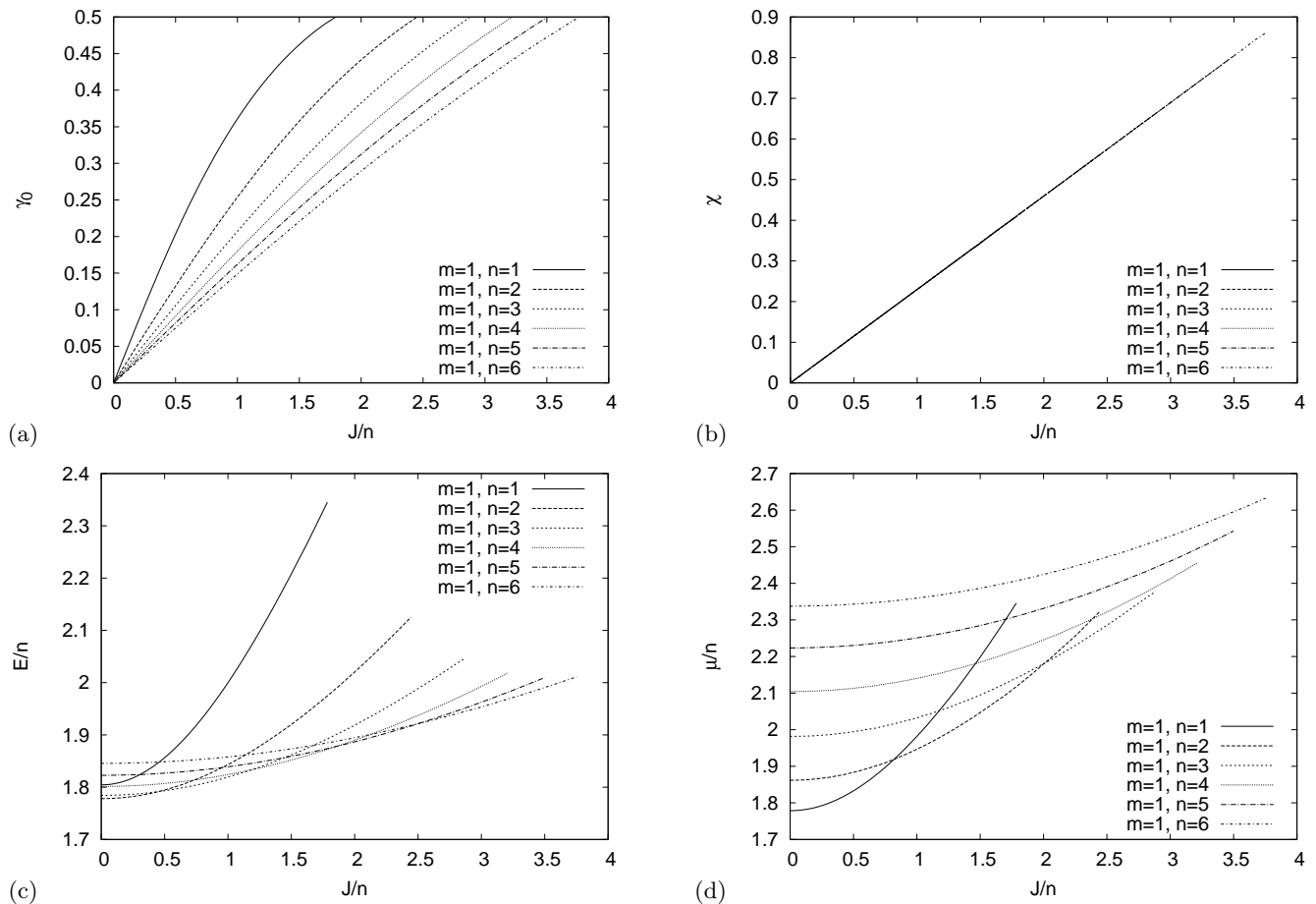


Figure 1: Properties of multisphaleron solutions ($m = 1, n = 1, \dots, 6$): (a) the asymptotic value of the $U(1)$ field $\tilde{\gamma} = \gamma/gv$, (b) the $U(1)$ charge parameter χ , (c) the mass per sphaleron E/n (in units of $E_0 = 4\pi v/g$), (d) the magnetic moment per sphaleron μ/n (in units of $\mu_0 = e/\alpha_W M_W$) versus the angular momentum per sphaleron J/n (in units of $J_0 = 4\pi/g^2$)

to the charge Q) versus the scaled angular momentum per sphaleron, J/n . We indeed observe a single straight line, which extends the further the greater n . Since the charge parameter has been extracted from the asymptotic fall-off of the $U(1)$ function a_1 , whereas the angular momentum has been obtained from the volume integral of the angular momentum density T_φ^t , this agreement reflects the good numerical quality of the solutions.

In Fig. 1c we present the energy of these solutions, which has been obtained from the volume integral of the energy density $-T_t^t$. For multisphalerons consisting of n sphalerons one expects that their energy should be of the order of n times the energy of a single sphaleron, thus E/n should be roughly constant. The deviations of the energy per sphaleron E/n from the energy of the single sphaleron can then be attributed to the interaction of the n sphalerons and be interpreted in terms of the binding energy of these multisphaleron configurations. For the employed value of the Higgs mass, we note that the static solutions with $n = 2 - 4$ represent bound states, since E/n is smaller than the energy of a single sphaleron, whereas the static solutions with $n > 4$ are slightly unbound [15].

When charge is added to these configurations and the solutions begin to spin, their energy increases monotonically with their angular momentum. The increase of the energy per sphaleron E/n with the angular momentum per sphaleron J/n is strongest for the branch of single sphaleron solutions. The more sphalerons a configuration consists of, the weaker is the increase of its energy per sphaleron E/n with increasing angular momentum per sphaleron J/n . Thus charge and rotation contribute relatively less to the total energy for these “many sphaleron” configurations (e.g. only 8% for $n = 6$ as compared to 30% for $n = 1$). Consequently, the rotating multisphaleron configurations turn into bound states beyond some critical value of the angular momentum.

Sphalerons possess a large magnetic moment μ . For multisphalerons consisting of n sphalerons one then expects that their magnetic moment should be roughly n times the magnetic moment μ of a single sphaleron. As seen in Fig. 1d, where we exhibit the magnetic moment per sphaleron μ/n versus the angular momentum per sphaleron J/n , this first guess is somewhat crude. For static configurations, the interaction between the sphalerons gives rise to a systematic (almost linear) increase of the magnetic moment per sphaleron μ/n with the number of sphalerons.

When charge and thus angular momentum is added to these configurations, their magnetic moment increases monotonically with increasing angular momentum. Again, this increase is strongest for the branch of single sphaleron solutions, and the increase is the weaker the more sphalerons a configuration consists of.

Having discussed the global properties of these solutions, we now turn to their local properties. In particular, we address the effect of the presence of charge and rotation on the energy density $-T_t^t$, and on the modulus of the Higgs field $|\Phi|$. As an example, we illustrate the energy density $-T_t^t$, the magnitude of the Higgs field $|\Phi|$, and the angular momentum density T_φ^t for an almost maximally rotating multisphaleron solution ($m = 1, n = 3, \tilde{\gamma} = 0.499$) in Fig. 2.

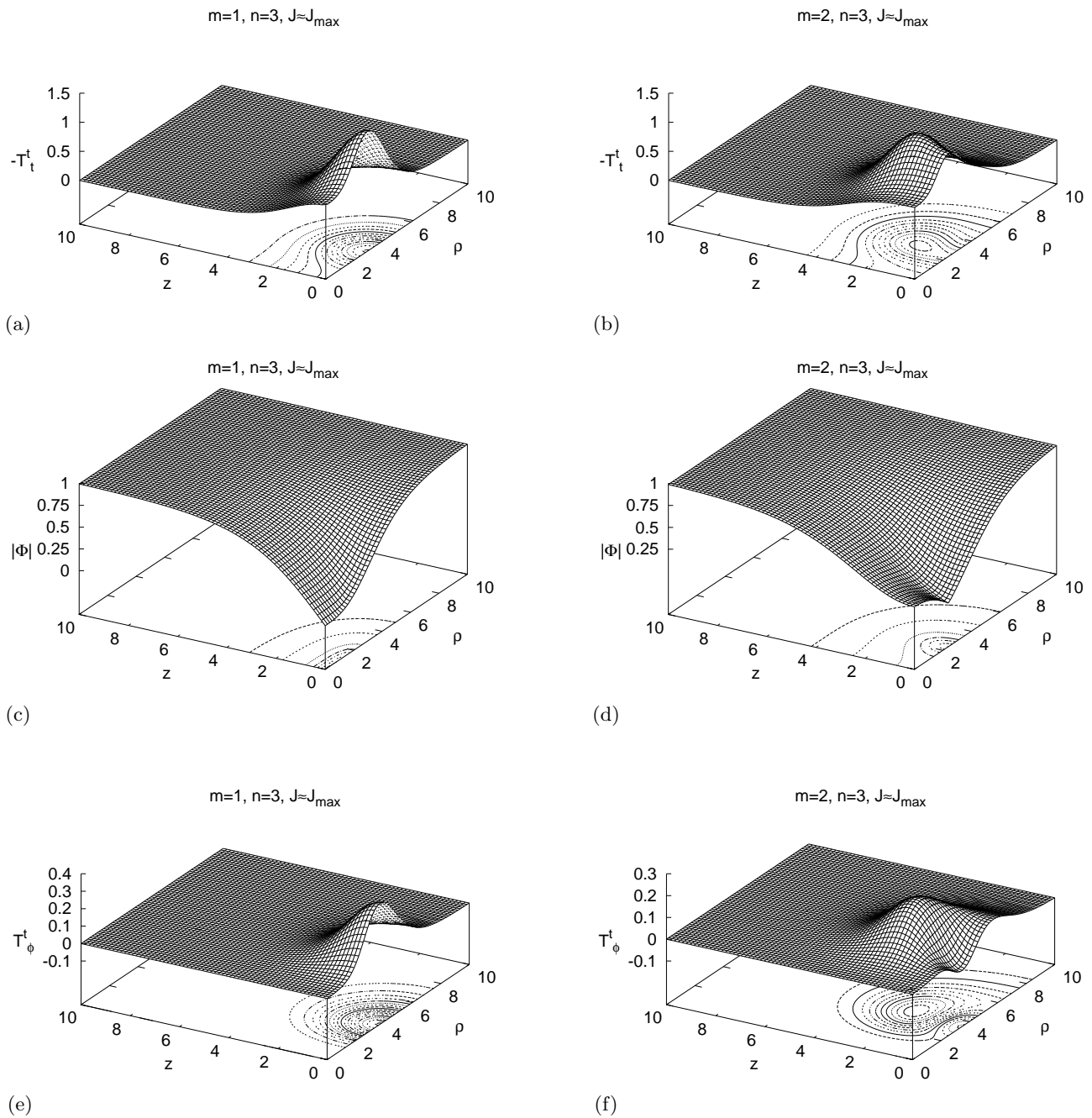


Figure 2: The energy density $-T_t^t$ (top), the modulus of the Higgs field $|\Phi|$ (middle), and the angular momentum density T_φ^t (bottom) are exhibited for an $m = 1, n = 3$ multisphaleron solution (left) and an $m = 2, n = 3$ sphaleron-antisphaleron system (right) close to maximal rotation.

In multisphalerons, the region with large energy density is torus-like, where its maximum is forming a ring in the equatorial plane. When we add electric charge and angular momentum to the static configuration, we observe that

the energy density is spreading further out, while at the same time its overall magnitude is reduced. Such a spreading of the energy density with increasing charge is also seen in dyons, for instance, and we attribute this effect to the presence of charge and the associated repulsion. Indeed, this spreading becomes quite pronounced for large values of the charge. The expected effect of the presence of angular momentum, on the other hand, is a centrifugal shift of the energy density. Indeed, we observe, that with increasing angular momentum the torus-like region of large energy density moves further outward to larger values of ρ .

The modulus of the Higgs field of the multisphaleron solutions has a single node at the origin, from where it starts to increase linearly in the direction of the symmetry axis, to reach its vacuum expectation value at infinity. In the equatorial plane, in contrast, the modulus of the Higgs field starts to increase from the origin much slower (i.e., only with power ρ^n). As the configurations are endowed with charge and rotation, the Higgs field hardly changes. Indeed, the effect of charge and rotation on the modulus of the Higgs field is barely noticeable, even at the maximal strength.

The angular momentum density for the multisphaleron solutions is torus-like and centered in the equatorial plane analogous to the energy density. However, the region of large angular momentum density is located further outwards at larger values of ρ , while it vanishes on the symmetry axis.

B. Sphaleron-antisphaleron systems

Let us now turn to sphaleron-antisphaleron systems. For $n = 1$ they represent sphaleron-antisphaleron chains, where m sphalerons and antisphalerons are located on the symmetry axis, in static equilibrium. For $n = 2$ the chain is formed from m multisphalerons and -antisphalerons, thus the modulus of the Higgs field still possesses only isolated nodes on the symmetry axis. However, as n increases further, the character of the solutions changes, and new types of configurations appear, where the modulus of the Higgs field vanishes on rings centered around the symmetry axis. Therefore we refer to these solutions as vortex ring solutions. We note, that the precise evolution of the isolated nodes on the symmetry axis and the vortex rings in the bulk with increasing n is sensitive to the value of the Higgs mass [20].

In the following we demonstrate the effect of charge and rotation on these sphaleron-antisphaleron systems by focussing on the configurations with $n = 3$ and $m = 1, \dots, 6$. The static solutions have been constructed before [20]. For the chosen parameters, the modulus of the Higgs field of the static $m = 2$ configuration vanishes only on a ring in the equatorial plane. The static $m = 3$ configuration has a node at the origin and in addition two rings, located symmetrically above and below the xy -plane. The static $m = 4$ configuration has only two symmetrical vortex rings. For $m = 5$, the two symmetrical vortex rings are supplemented by a node at the origin, and for $m = 6$ two symmetrical vortex rings and two inner nodes on the symmetry axis are present.

Again we first discuss the global properties of these solutions, following the above scheme. Since only the integer n (but not m) enters the relation between the charge and the angular momentum, we continue to show all quantities versus the scaled relative angular momentum J/n . We exhibit in Fig. 3a the dependence of the asymptotic gauge field parameter $\tilde{\gamma} = \gamma/gv$ on the scaled relative angular momentum J/n for the configurations with $n = 3$ and $m = 1, \dots, 6$. As before, at the maximal value $\tilde{\gamma}_{\max} = 1/2$ the solutions have maximal angular momentum. Moreover, we observe that the maximal value of the relative angular momentum J_{\max}/n increases with m . Thus the higher the number of constituents a configuration (i.e., the product mn), the more angular momentum each of the constituents can contribute.

In Fig. 3b we demonstrate that the linear relation (19) between the charge Q and the angular momentum J is well satisfied also by the numerically constructed sphaleron-antisphaleron systems. We again obtain a single straight line, when exhibiting the charge versus the relative angular momentum J/n , which extends the further the greater n .

Addressing the energy of these solutions, we expect that it should be roughly proportional to the number mn of constituents of the configurations. We therefore consider the relative energy E/mn , i.e., the energy per constituent. The deviations of E/mn from the energy of a single sphaleron can then be attributed to the interaction of the sphalerons and antisphalerons in the system and be interpreted in terms of their binding energy. We present the relative energy E/mn of these solutions in Fig. 3c. We note that the binding energy increases with an increasing number of constituents. Also, the increase of the energy per constituent E/mn with J/n is the stronger the smaller the number of constituents. Charge and rotation contribute therefore relatively less to the total energy for the “many constituents” configurations.

Addressing finally the magnetic moment μ of these solutions, we also consider the magnetic moment per constituent μ/mn . As seen in Fig. 3d, the interaction between the constituents gives rise to a decrease of the magnetic moment per constituent μ/mn with increasing m .

Now we turn to the local properties of these sphaleron-antisphaleron systems. As examples, we exhibit the $m = 2$, $n = 3$ system in Fig. 2 (right column) and the $m = 3$, $n = 3$ and $m = 4$, $n = 3$ systems in Fig. 4, where we again display the energy density, the modulus of the Higgs field and the angular momentum density for solutions close to maximal rotation.

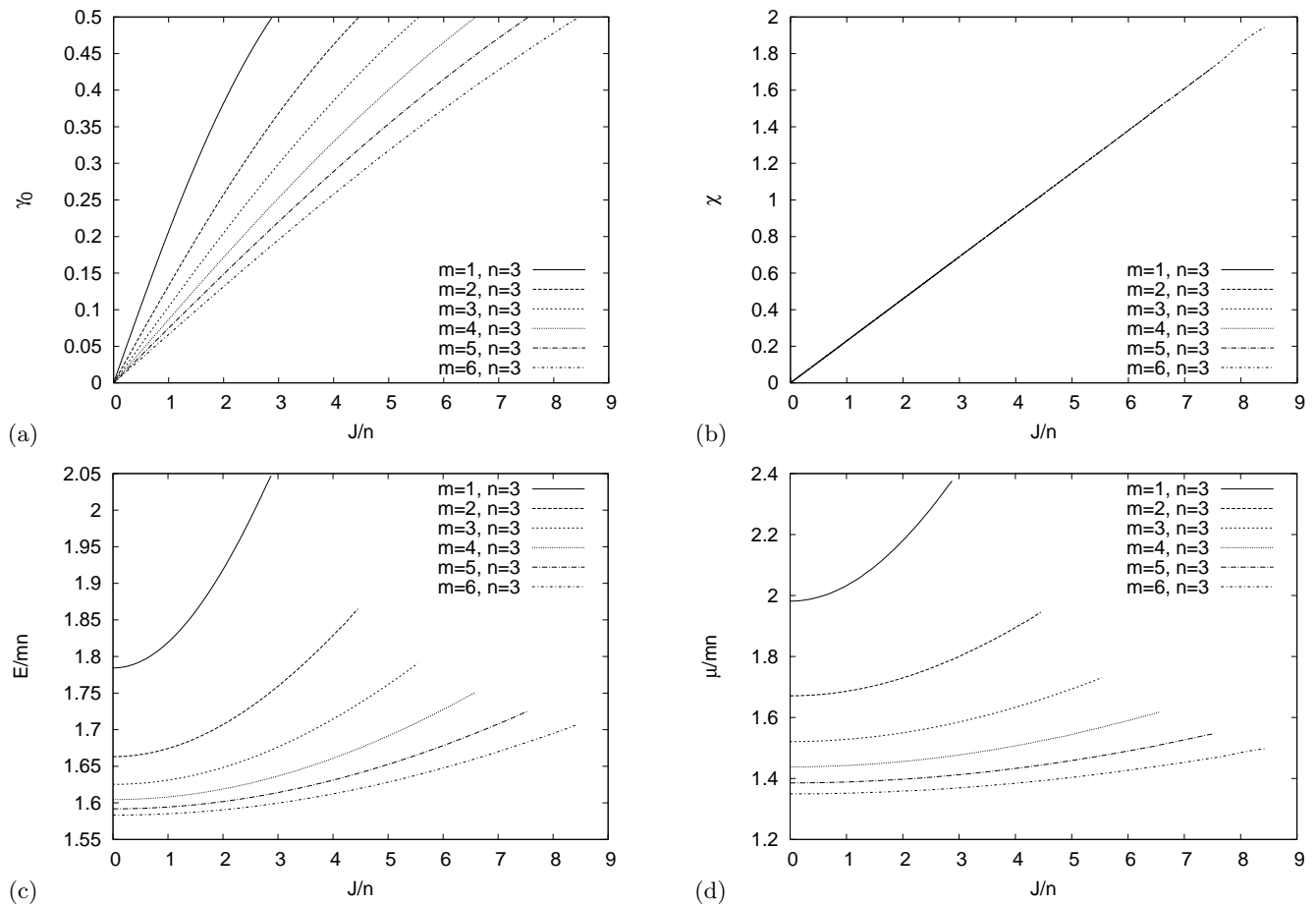


Figure 3: Same as Fig.1 for sphaleron-antisphaleron systems ($m = 1, \dots, 6, n = 3$).

Only in sphaleron-antisphaleron pairs and chains with $n = 1$ the regions with large energy density are localized around the Higgs field nodes on the symmetry axis. In all other sphaleron-antisphaleron systems, the regions with large energy density are torus-like, where a configuration may possess several such tori. The location and number of these tori depends on the numbers m and n and on the parameters, just as the nodes of the Higgs field are determined by these quantities.

As for the multisphalerons, the effect of the presence of electric charge is that the energy density spreads further out, while at the same time its overall magnitude reduces. Likewise, the effect of the presence of angular momentum is a centrifugal shift of the energy density. With increasing angular momentum the torus-like regions of large energy density move further outward to larger values of ρ .

The modulus of the Higgs field of the sphaleron-antisphaleron systems changes very little and is barely noticeable, even when the systems carry maximal charge and angular momentum.

The angular momentum density of the sphaleron-antisphaleron systems is also characterized by the presence of tori. But it contains tori of large positive angular momentum density as well as negative angular momentum density. The tori of the angular momentum density are spatially related to the tori of the energy density. In particular, the location of the positive tori is associated with the location of the tori of the energy density, with the negative tori inbetween.

C. Equilibrium condition

Finally, we would like to address the question of the equilibrium of such composite configurations as sphaleron-antisphaleron pairs and more general sphaleron-antisphaleron systems. As discussed previously [31–33], a necessary

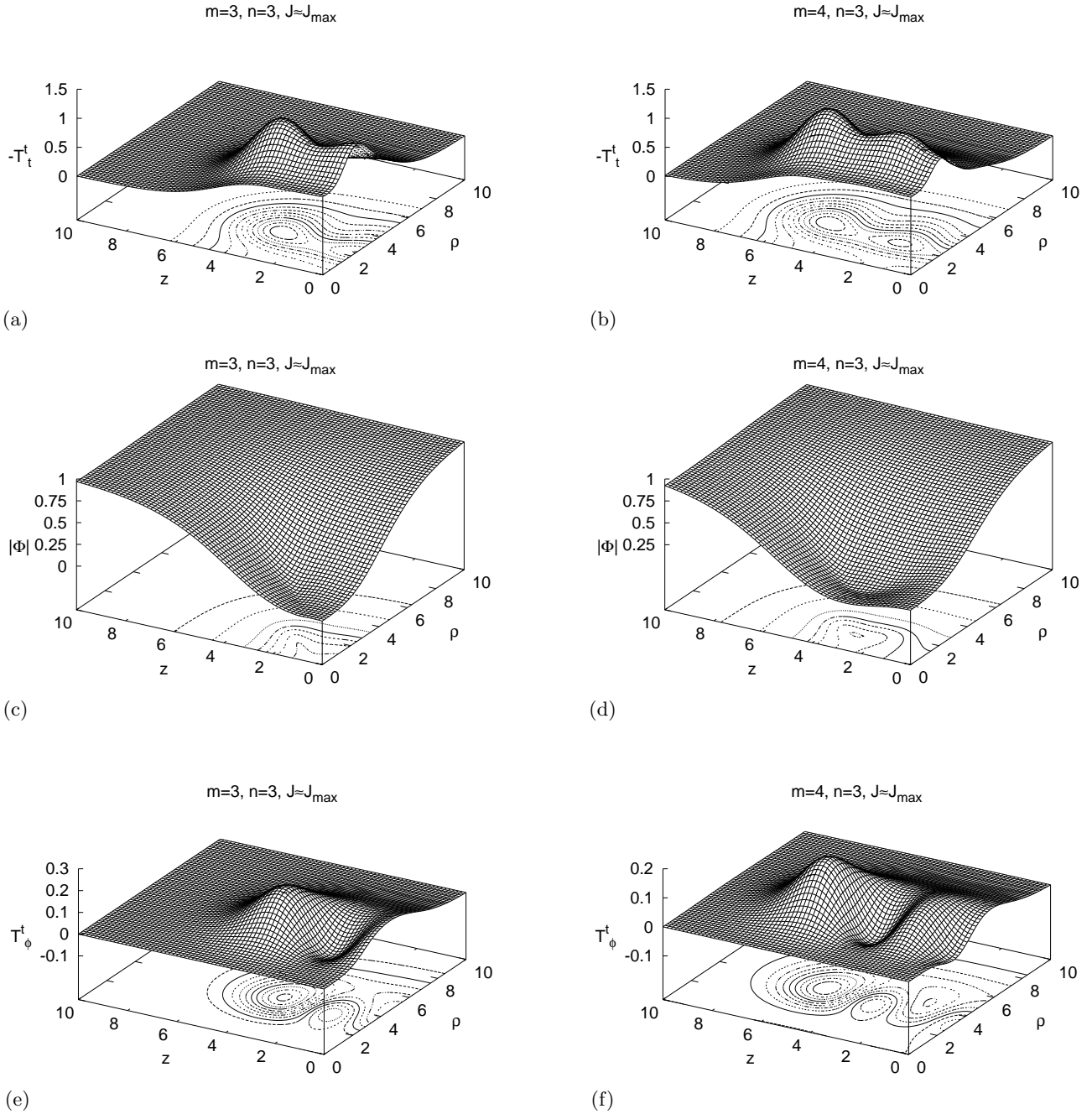


Figure 4: Same as Fig.2 for the sphaleron-antisphaleron systems $m = 3, n = 3$ (left) and $m = 4, n = 3$ (right).

condition for the equilibrium of such axially symmetric configurations is

$$\int_S T_{zz} dS = 0 \quad (26)$$

where T_{zz} is the respective component of the stress energy tensor and S is the equatorial plane. When this condition is satisfied, the net force between the constituents in the upper and in the lower hemisphere vanishes, thus yielding equilibrium. If T_{zz} vanishes everywhere in the equatorial plane, this condition is met trivially, if on the other hand T_{zz} does not identically vanish, the various contributions to the surface integral (26) must precisely cancel each other.

To understand how the equilibrium condition is satisfied in these sphaleron-antisphaleron systems, we have extracted the T_{zz} component of the stress energy tensor. We illustrate T_{zz} for two rather different configurations in Fig. 5. In

Fig. 5a we display T_{zz} for the static sphaleron-antisphaleron pair in the upper hemisphere. In the equatorial plane T_{zz} appears to almost vanish. We therefore focus on the equatorial plane in Fig. 5c. Here T_{zz} is small, but finite (except when it changes sign). To gain further insight into how the equilibrium results from the various forces present in the system, we consider the contributions from the respective parts of the Lagrangian separately. We exhibit these also in Fig. 5c. We note, that the positive contribution from the $SU(2)$ gauge field part almost cancels the negative contributions from the $U(1)$ and Higgs parts, yielding in total a T_{zz} which is almost but not quite vanishing in the equatorial plane. In the inner region the total T_{zz} is slightly positive, while in the outer region it is slightly negative, yielding together a vanishing surface integral (26), within the numerical accuracy.

The situation is similar for the sphaleron-antisphaleron chain, consisting of four constituents ($m = 4, n = 1$). Also, the inclusion of rotation does not change this overall behaviour of these types of solutions. For most other systems, however, T_{zz} does not nearly vanish in the equatorial plane. This is exhibited exemplarily in Fig. 5b for the fast rotating sphaleron-antisphaleron system with $m = 4, n = 3$. The features of T_{zz} seen here, are very typical, and hardly change with rotation, since the effect of rotation is basically a slight shift in magnitude. However, while T_{zz} is rather large in the equatorial plane for these configurations, its positive and negative contributions to the surface integral do cancel as required for equilibrium.

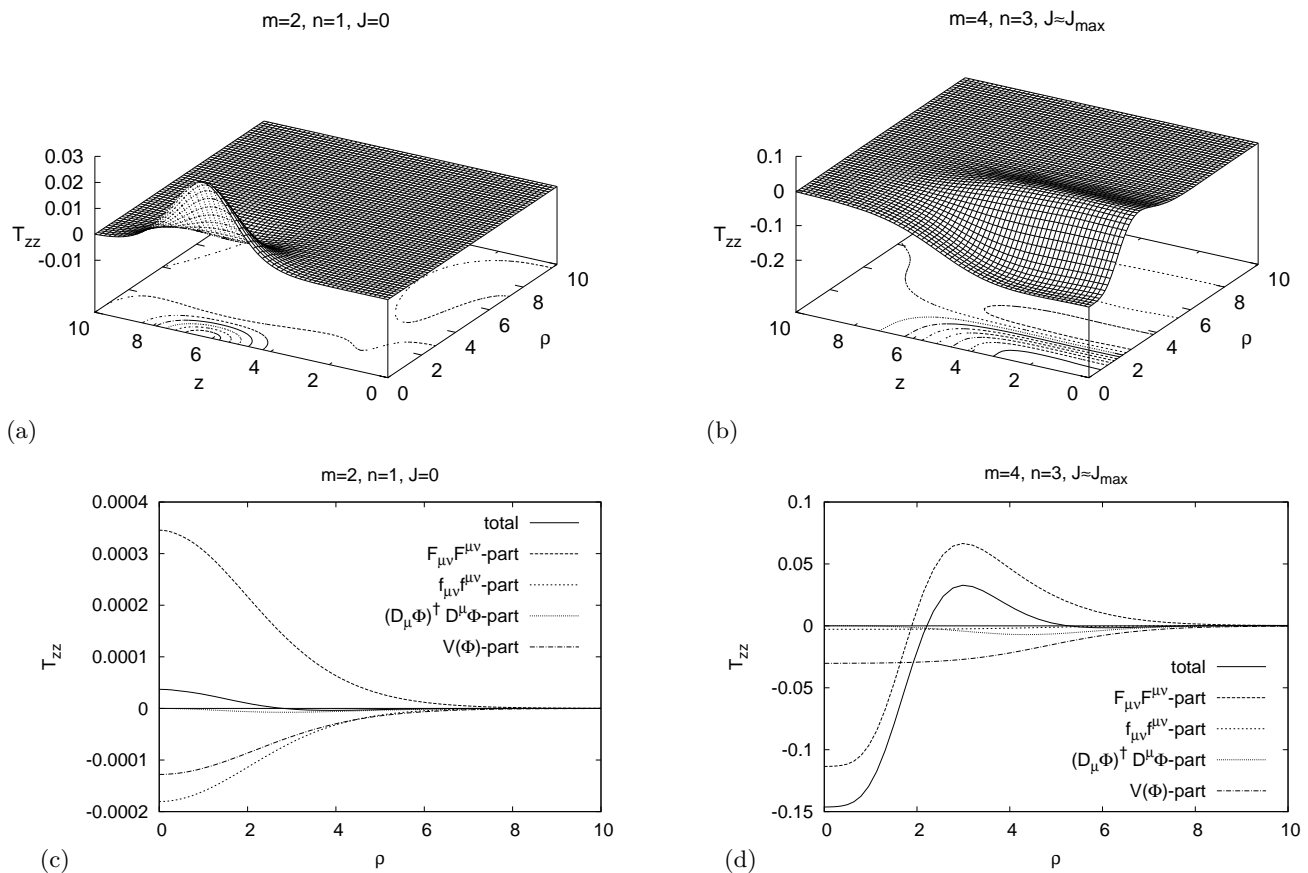


Figure 5: The full stress-energy component T_{zz} (upper) and its $SU(2)$, $U(1)$, Higgs covariant derivative and Higgs potential parts in the equatorial plane (lower) for the sphaleron-antisphaleron systems $m = 2, n = 1, J = 0$ (left) and $m = 4, n = 3, J \approx J_{\max}$ (right).

V. CONCLUSIONS

We have considered sphaleron-antisphaleron pairs, chains and vortex ring solutions in Weinberg-Salam theory, which are characterized by two integers n and m . Starting from the respective neutral electroweak configurations, we have obtained the corresponding branches of rotating electrically charged solutions. These branches exist up to maximal values of the charge and angular momentum, beyond which localized solutions are no longer possible.

The angular momentum J and the charge Q of these sphaleron-antisphaleron systems are proportional

$$J = nQ/e.$$

Their energy and binding energy increase with increasing rotation, and so does their magnetic moment. With increasing charge the energy density of the configurations spreads further out, while its overall magnitude reduces. At the same time the effect of the rotation is a centrifugal shift of the energy density tori to larger radii.

We have also addressed the equilibrium condition (26) for these sphaleron-antisphaleron systems. In all systems, it is the surface integral that vanishes to give equilibrium, and not the stress-energy tensor component T_{zz} by itself. However, for the sphaleron-antisphaleron pair (and other even m chains) the stress-energy tensor component T_{zz} almost vanishes in the equatorial plane. In these configurations the positive contribution from the $SU(2)$ part almost cancels the negative contributions from the $U(1)$ and Higgs parts, thus yielding an almost vanishing total T_{zz} in the equatorial plane.

The next step will be to study the fermion modes in the background of such rotating electroweak configurations to understand their relevance for baryon number violating processes [34]. Moreover it will be interesting to include the effect of gravitation [35] to obtain rotating gravitating regular configurations as well as black hole solutions.

Acknowledgement: We gratefully acknowledge discussions with G. Gibbons, E. Radu and M. S. Volkov. R.I. acknowledges support by the Volkswagen Foundation, and B.K. support by the DFG.

-
- [1] N. S. Manton, Phys. Rev. D **28**, 2019 (1983).
 - [2] F. R. Klinkhamer and N. S. Manton, Phys. Rev. D **30**, 2212 (1984).
 - [3] B. Kleihaus, J. Kunz and Y. Brihaye, Phys. Lett. B **273**, 100 (1991).
 - [4] J. Kunz, B. Kleihaus and Y. Brihaye, Phys. Rev. D **46**, 3587 (1992).
 - [5] G. 't Hooft, Phys. Rev. Lett. **37**, 8 (1976).
 - [6] A. Ringwald, Nucl. Phys. B **330**, 1 (1990).
 - [7] L. D. McLerran, Acta Phys. Polon. B **25**, 309 (1994) [arXiv:hep-ph/9311239].
 - [8] V. A. Rubakov and M. E. Shaposhnikov, "Electroweak baryon number non-conservation in the early universe and in Usp. Fiz. Nauk **166**, 493 (1996) [Phys. Usp. **39**, 461 (1996)] [arXiv:hep-ph/9603208].
 - [9] M. Dine and A. Kusenko, Rev. Mod. Phys. **76**, 1 (2004) [arXiv:hep-ph/0303065].
 - [10] F. R. Klinkhamer and C. Rupp, J. Math. Phys. **44**, 3619 (2003) [arXiv:hep-th/0304167].
 - [11] P. M. Saffin and E. J. Copeland, Phys. Rev. D **57**, 5064 (1998) [arXiv:hep-ph/9710343].
 - [12] E. Radu and M. S. Volkov, Phys. Rev. D **79**, 065021 (2009) [arXiv:0810.0908 [hep-th]].
 - [13] B. Kleihaus, J. Kunz and M. Leissner, Phys. Lett. B **678**, 313 (2009) [arXiv:0810.1142 [hep-ph]].
 - [14] B. Kleihaus and J. Kunz, Phys. Lett. B **329**, 61 (1994) [arXiv:hep-ph/9403289].
 - [15] B. Kleihaus and J. Kunz, Phys. Rev. D **50**, 5343 (1994) [arXiv:hep-ph/9405387].
 - [16] Y. Brihaye and J. Kunz, Phys. Rev. D **50**, 4175 (1994) [arXiv:hep-ph/9403392].
 - [17] F. R. Klinkhamer, Z. Phys. C **29**, 153 (1985).
 - [18] F. R. Klinkhamer, Phys. Lett. B **246**, 131 (1990).
 - [19] F. R. Klinkhamer, Nucl. Phys. B **410**, 343 (1993) [arXiv:hep-ph/9306295].
 - [20] B. Kleihaus, J. Kunz and M. Leissner, Phys. Lett. B **663**, 438 (2008) [arXiv:0802.3275 [hep-th]].
 - [21] B. Kleihaus, J. Kunz and Y. Shnir, Phys. Lett. B **570**, 237 (2003) [arXiv:hep-th/0307110].
 - [22] B. Kleihaus, J. Kunz and Y. Shnir, Phys. Rev. D **68**, 101701 (2003) [arXiv:hep-th/0307215].
 - [23] B. Kleihaus, J. Kunz and Y. Shnir, Phys. Rev. D **70**, 065010 (2004) [arXiv:hep-th/0405169].
 - [24] J. J. Van der Bij and E. Radu, Int. J. Mod. Phys. A **17**, 1477 (2002) [arXiv:gr-qc/0111046].
 - [25] B. Kleihaus, J. Kunz and F. Navarro-Lerida, Phys. Rev. Lett. **90**, 171101 (2003) [arXiv:hep-th/0210197].
 - [26] M. S. Volkov and E. Wahnert, Phys. Rev. D **67**, 105006 (2003) [arXiv:hep-th/0302032].
 - [27] E. Radu and M. S. Volkov, Phys. Rept. **468**, 101 (2008) [arXiv:0804.1357 [hep-th]].
 - [28] B. Kleihaus, J. Kunz, F. Navarro-Lerida and U. Neemann, Gen. Rel. Grav. **40**, 1279 (2008) [arXiv:0705.1511 [gr-qc]].
 - [29] B. Kleihaus, J. Kunz and K. Myklevoll, Phys. Lett. B **582**, 187 (2004) [arXiv:hep-th/0310300].
 - [30] W. Schönauer and R. Weiß, J. Comput. Appl. Math. **27**, 279 (1989).
 - [31] Y. Aharonov, A. Casher, S. R. Coleman and S. Nussinov, Phys. Rev. D **46**, 1877 (1992).
 - [32] R. Beig and R. M. Schoen, Class. Quant. Grav. **26**, 075014 (2009) [arXiv:0811.1727 [gr-qc]].
 - [33] R. Beig, G. W. Gibbons and R. M. Schoen, Class. Quant. Grav. **26**, 225013 (2009) [arXiv:0907.1193 [gr-qc]].
 - [34] J. Kunz and Y. Brihaye, Phys. Lett. B **304**, 141 (1993) [arXiv:hep-ph/9302313].
 - [35] R. Ibadov, B. Kleihaus, J. Kunz and M. Leissner, Phys. Lett. B **663**, 136 (2008) [arXiv:0802.3335 [gr-qc]].
 - [36] The exponent arises as a combination from the mass term, obtained from the Higgs vacuum expectation value, and the non-Abelian gauge field interaction term, and yields asymptotically an exponential decay with decay constant proportional to $\sqrt{1 - 4\tilde{\gamma}^2}$.